Wavelet preprocessing for lessening truncation effects in nearfield acoustical holography

Jean-Hugh Thomas[a] and Jean-Claude Pascal[b]
Laboratoire d'Acoustique de l'Université du Maine, LAUM UMR-CNRS 6613, Avenue Olivier Messiaen 72085 Le Mans Cedex 09, France

(Received 22 July 2004; revised 31 March 2005; accepted 11 May 2005)

The goal of planar nearfield acoustical holography (NAH) is to recover the sound field at the sound source from pressure measurements made close to the source plane. The theory requires the pressure to be measured over a complete plane. Because experimentation consists of acquiring only a finite measurement aperture of the pressure field, it naturally causes erroneous values in the reconstructed field. Wavelet preprocessing applied to the pressure measurements in the nearfield provides a solution to lessen the effects due to the truncation of the hologram. The approach is based on a multiresolution analysis of the field from different wave number bands followed by selective spatial filtering of effects highlighted by the first analysis. Experimental results show the relevance of the method by comparison to standard NAH involving exponential filtering in the wave number domain. The computation of objective indicators based on distance measurements between wave number spectra and comparisons between patterns composed of relevant features drawn from experimental data are proposed to give objective criteria to prove the viability of the method. © *2005 Acoustical Society of America.* [DOI: 10.1121/1.1945469]

PACS number(s): 43.60.Sx, 43.60.Hj, 43.60.Pt [EGW] Pages: 851–860

I. INTRODUCTION

The aim of planar nearfield acoustical holography (NAH) is to reconstruct the sound field at the sound source from pressure measurements made close to the source plane. These measurements are carried out using an array of microphones or a single microphone moving across a finite size grid when the acoustic noise is stationary. Thus holography is applied to a truncated acoustic measurement field, which causes erroneous values in the reconstructed pressure field. Indeed, the discontinuity in the acquired pressure field increases the distortions of the usual reconstruction procedure due to the exponential amplification of the evanescent waves in the wave number spectrum. The goal of our study is to lessen the effects of the truncation of the hologram in planar NAH. A wavelet method is used for this purpose. Full details of the approach are given in the first part of the paper. In the second part, some indicators are proposed to compare results obtained by standard NAH and by NAH coupled with the wavelet preprocessing. The aim of this part is to prove the relevance of the method discussed, from objective criteria computed from the wave number spectra involved.

Several authors have already worked on the lessening of truncation effects. A weighting window is proposed[1] but it has the disadvantage of adding distortions when the gradient of the rebuilt pressure field is to be used to calculate the acoustical and structural intensity. Some authors have applied regularization approaches to NAH problems, based on the singular value decomposition (SVD) of the matrix which relates the normal velocity of the vibrating surface to the hologram pressure on the measurement plane.[2–4] Williams, in particular, presented a comparative study of regularization methods such as the Tikhonov procedure, the Landweber iteration, and the conjugate gradient approach.[5] In his application, he underlined the fact that the Veronesi filter,[6] or exponential filter, provided the best results, even in comparison with a modified Tikhonov approach, improving the results given by the three tested methods. That is why the approach using wavelet processing, presented in the paper, is compared to NAH with the use of the Veronesi filter as a regularization tool. The advantages of these regularization methods are that they process automatically and can be used for planar, cylindrical, and spherical geometries. Tikhonov regularizations in conjunction with a parameter-choice method [L-curve criterion or the generalized cross-validation method (GCV)] are also successfully used for reconstructing acoustic sources using the inverse boundary element method (IBEM)[7] or, more recently, hybrid NAH based on a modified Helmholtz equation least-squares (HELS) method.[8] Another approach consisted in reconstructing the pressure field of the source plane over an area larger than the small region, or "patch," where the pressure was measured.[9,10] The starting point of the method is the measurement plane, i.e., the hologram, extended by zero-padding to the size needed for the pressure field of the source plane. The idea is to reconstruct the pressure field on the source plane and then to propagate the latter to the measurement plane. The central part, whose dimension is the same as that of the patch, is replaced by the hologram and the process reiterates until the field propagated is similar to the hologram. The method seems to give interesting results even though it needs many iterations. Other techniques which accurately calculate the spatial derivatives in the wave number domain[11,12] cannot be employed in backward propagation because they limit the width or modify the shape of the k spectrum.

[a]Electronic mail: jean-hugh.thomas@univ-lemans.fr
[b]Electronic mail: jean-claude.pascal@univ-lemans.fr

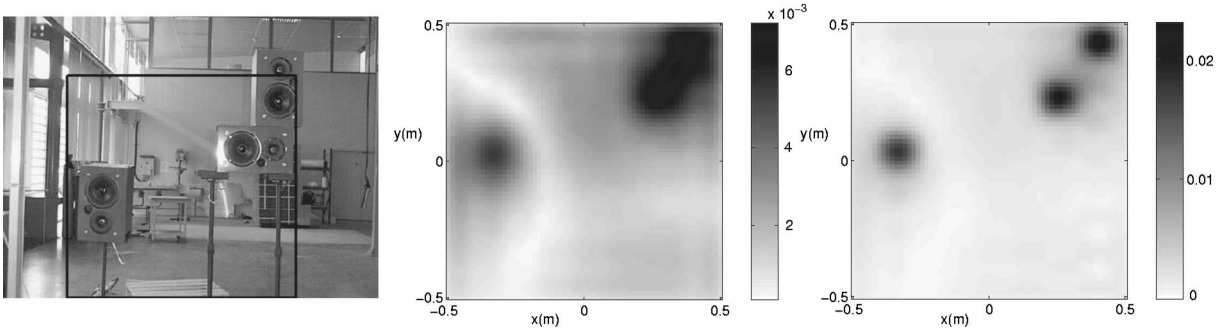

FIG. 1. The experiment with three loudspeakers in a vertical plane and a square frame is shown left. The 16×16 pressure field A_0 (center), measured from this frame, 10 cm from the source plane, is the starting point of the study. The pressure field directly acquired 1 cm from the source plane on the right is the reference field intended to be reconstructed from the image in the center using NAH with the wavelet preprocessing.

The approach discussed in the paper does not belong to regularization-based methods but involves multiresolution decomposition of the acoustical field. The aim of this analysis is to highlight truncation effects that appear at different resolutions. Once the effects have been located, they are selectively filtered. To our knowledge, El Khoury and Nouals were the first to propose this two-step method.[13] The stages of the method are as follows: multiresolution analysis and selective spatial filtering are described in Sec. III. The selective spatial filtering we proposed is, in particular, different from the Hamming window used by El Khoury and Nouals.[13] The wavelet processing is also presented from a wave number point of view: each decomposition of the acoustic field at one resolution involves specific wave number filtering, highlighted in Sec. III. Section IV describes the results obtained using the proposed wavelet method to experimentally reconstruct acoustic fields very near the source plane. The experimental configuration tested here involves a three-monopole point source plane that has already been tested successfully on simulated cases.[14] Several figures, illustrating back-propagated acoustic fields, are also displayed to compare results obtained from standard NAH and from NAH coupled with wavelet preprocessing. Because it is sometimes difficult to make visual comparisons of processing results in acoustic imaging, we propose in Sec. V to use objective indicators to prove the relevance of the wavelet method for NAH. First the wave number spectra resulting from standard NAH and from wavelet processing are compared to a reference spectrum through the computation of a similarity indicator between the spectra, which is based on distance measurements. The smallest distance gives the most relevant spectrum. Second, a pattern recognition approach is used: several features are extracted from the wave number spectra to create a pattern which may be then represented by a point in the feature space. Each method gives a pattern whose location in the feature space is compared to that of a reference pattern. The closer the pattern is to the reference, the more relevant the source reconstruction. As the steps of the proposed method are illustrated all along the paper by images of the experimental acoustic fields, the paper starts in Sec. II with a description of the experiment and explains the principle of the study.

II. DESCRIPTION OF THE STUDY AND THE EXPERIMENT

The experimental configuration for the holographic measurements consisted of three stationary loudspeakers excited in a vertical plane (Fig. 1). Two of them were close to each other. The pressure was measured 10 cm from the source plane on a square grid of 28×28 points. The scan was conducted in an automated point-by-point fashion using a single microphone. The complex pressure was retrieved from the phase relations between the acquired acoustic signals and the excitation signal. The step size in both x and y directions was $\Delta L=6.7$ cm, providing an overall scan dimension of 1.8×1.8 m^2. The study focuses on a smaller surface of 16×16 points located at the center of this area (see the black square frame in the picture in Fig. 1). This region, which measured 1.0×1.0 m^2, was chosen so that the highest loudspeaker was very near its border, resulting in unsatisfactory values in the reconstruction processing. The wavelength and the wave number of the stationary sources being studied are respectively $\lambda=0.85$ m and $k_0=2\pi/\lambda=7.4$ rad m^{-1} at the frequency of 400 Hz. The aim of our experiment is to reconstruct an acoustic field 1 cm from the source plane, from the acquired acoustic field 10 cm from the loudspeaker plane. From the experiment shown on the left in Fig. 1, the 16×16-point pressure field in the center, acquired 10 cm from the sources, is back-propagated 1 cm from the source plane using NAH. The pressure field resulting from the method discussed in the paper is expected to be similar to the reference one on the right directly acquired 1 cm from the source plane. These fields, as throughout the paper, are interpolated on a 64×64 grid using the Shannon interpolation from the computed fields on a 16×16 grid, giving sharper images.

The wavelet method,[13–15] which is both space and frequency selective, involves modifying the acquired acoustic pressure field before solving the holography inverse problem (NAH) as shown by the synopsis in Fig. 2. The method differs from the standard one in that it does not apply any filtering in the wave number spectrum after the Fourier transform. However, there is no denying that the wavelet preprocessing itself filters the data in the wave number domain. The aim of the next section is to explain how the acquired pressure field is modified by the wavelet method and in particular how its wave number spectrum is affected.

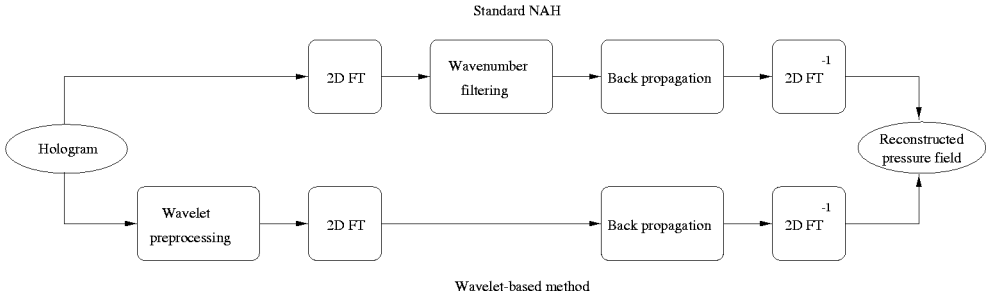

FIG. 2. Synopsis of the wavelet-based method and the standard holography. 2D FT denotes the two-dimensional Fourier transform and 2D FT^{-1} its inverse.

III. A WAVELET PREPROCESSING METHOD

A. Principle

The first stage is based on a multiresolution analysis[16] of the acquired pressure field 10 cm from the source plane. It provides subimages highlighting different characteristics of the pressure field according to a given resolution, in particular the edges caused by the finite size of the acoustic field. The main advantage of decomposition (which is used in data compression with MPEG video compression standards) is that the image studied may be reconstructed from the subimages, using a simple algorithm involving zero insertion and summation.

The second stage of the method is based on selective spatial filtering of the edges highlighted by the multiresolution analysis. The spatial filter is a Π-modified function which was devoted to pattern recognition applications[17] as a model of class membership function. Here it is applied to the subimages. Then the resulting subimages are added, yielding a modified pressure field to be used as an input of the holography algorithm.

B. Multiresolution analysis

In this part, multiresolution analysis is essentially presented in a physical sense as a filter bank analysis without the theory of wavelet bases which is reported in detail in the literature.[16,18] The method consists in analyzing a signal or an image at several resolutions. First it focuses on details, then it gives increasingly coarse approximations of the signal studied.

The decomposition of 1-D signals at one resolution involves a high-pass filter and a low-pass filter to separate the input signals into two components: an approximate and a detailed signal. At the first resolution, for 1-D signals sampled at frequency f_e, the high-pass filter extracts details in the $[f_e/4, f_e/2]$ band and the low-pass filter gives an approximation in the $[0, f_e/4]$ band. At the second resolution and so on, this two-step processing is reiterated on the approximation given from the previous resolution. At resolution j, the high-pass filter extracts details in the $[f_e/2^{j+1}, f_e/2^j]$ band and the low-pass filter gives an approximation in the $[0, f_e/2^{j+1}]$ band.

For images, the approach is similar except that the filters operate on the lines and the columns, involving four filtering operations instead of two. In this way, the first resolution wavelet analysis of A_0, the acquired pressure field 10 cm from the source plane, yields the four subimages A_1, H_1, V_1, and D_1 of Fig. 3 such that

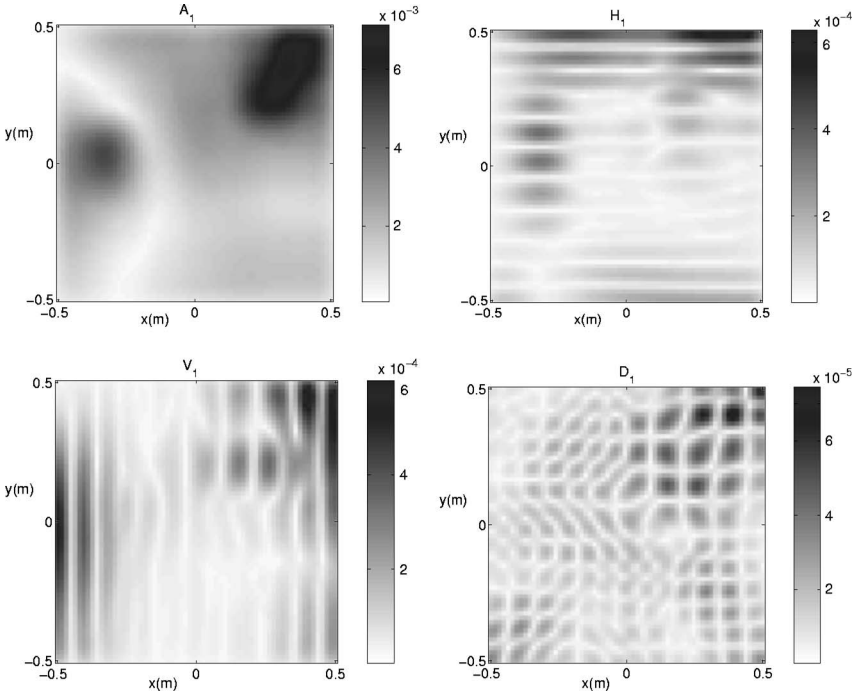

FIG. 3. Resulting acoustic fields (magnitude) without detail top left (A_1), with the horizontal edges top right (H_1), the vertical edges bottom left (V_1), and the corners bottom right (D_1) from a one-level multiresolution analysis of the acquired radiated field (A_0) in Fig. 1. The analysis is based on a Daubechies wavelet with eight vanishing moments.

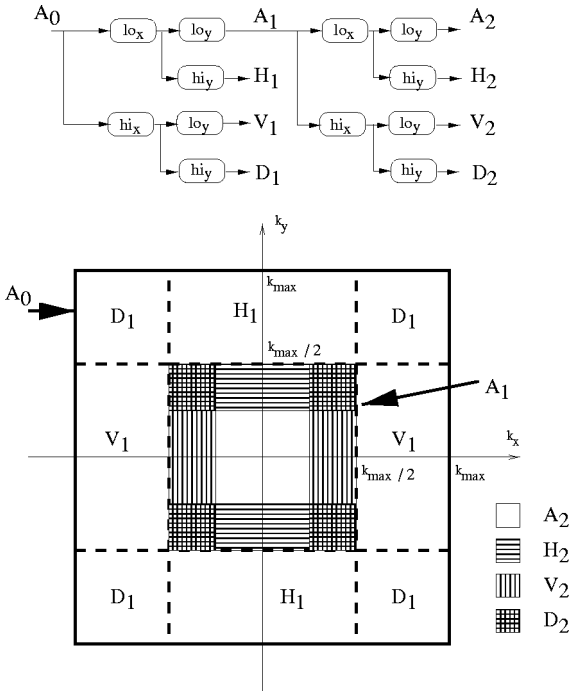

FIG. 4. Multiresolution analysis at level 2 from a wave number spectrum point of view: the original image A_0 is decomposed into seven subimages H_1, V_1, D_1, A_2, H_2, V_2, and D_2 using high-pass filtering (hi) and low-pass filtering (lo) horizontally (subscript x) or vertically (subscript y). The whole wave number domain of the acoustic field A_0, represented by a square of size k_{max}, is divided into several areas, each of them corresponding to a specific wave number band.

$$A_0 = A_1 + H_1 + V_1 + D_1. \tag{1}$$

The analysis highlights different components of the acoustic field as shown by analyzing wavelet processing in the wave number domain. Indeed, a j-resolution analysis of an acoustic field leads to filtering in the wave number space known as k space (see bottom part in Fig. 4):

(i) in the $[0, k_{max}/2^j]$ band in both directions k_x and k_y to obtain the approximation A_j (k_x and k_y are respectively wave numbers in x and y directions),

(ii) in the $[0, k_{max}/2^j]$ band in the k_x direction and in the $[k_{max}/2^j, k_{max}/2^{j-1}]$ band in the k_y direction to obtain image H_j highlighting the horizontal edges due to high-pass filtering on the vertical axis,

(iii) in the $[k_{max}/2^j, k_{max}/2^{j-1}]$ band in the k_x direction and in the $[0, k_{max}/2^j]$ band in the k_y direction to obtain image V_j highlighting the vertical edges due to high-pass filtering on the horizontal axis,

(iv) in the $[k_{max}/2^j, k_{max}/2^{j-1}]$ band in both directions k_x and k_y to obtain image D_j providing the details,

with $k_{max} = \pi/\Delta L$, the wave number limit due to space sampling ΔL.

In this approach, filtering is done on the lines, then on the columns or both on the lines and the columns (see top part in Fig. 4) while standard holography uses a unique circular filter that retains only wave numbers smaller than a k space cutoff k_c.

Figure 3 shows that features due to hologram truncation are spatially localized near the boundaries of the radiated field (see in particular the dark horizontal lines on image H_1 and the dark vertical lines on image V_1). Note that multiresolution analysis is performed using Daubechies wavelets computed from finite impulse responses of filters with 16 coefficients given in Ref. 16.

C. Selective spatial filtering

The aim is to remove the features due to the finite aperture of the antenna, emphasized by multiresolution analysis. Several standard windows (Hamming, Kaiser,…) can be used at this stage, but they generally have the disadvantage of reducing the area of the acquired acoustic field. Thus a two-dimensional Π-modified function Π_m shown in Fig. 5 and defined in 1-D by Eq. (2) is used: its shape is easily adjustable by changing two parameters λ and β. β sets the length of the top of the function and λ its slope:

$$\Pi_m(x,\lambda,\beta) = \begin{cases} 2\left(1 - \dfrac{x^2-\beta}{\lambda}\right)^2 & \text{if } \dfrac{\lambda}{2} + \beta \leqslant x^2 \leqslant \lambda + \beta, \\ 1 - 2\dfrac{[x^2-\beta]^2}{\lambda^2} & \text{if } \beta \leqslant x^2 \leqslant \dfrac{\lambda}{2} + \beta, \\ 1 & \text{if } 0 \leqslant x^2 \leqslant \beta, \\ 0 & \text{otherwise.} \end{cases} \tag{2}$$

The Π-modified functions of Fig. 5 are applied to the subimages provided by multiresolution analysis to filter the horizontal edges in the y direction, the vertical edges in the x direction, and the corners in both directions with a polar shape. Only the approximate subimage remains unchanged.

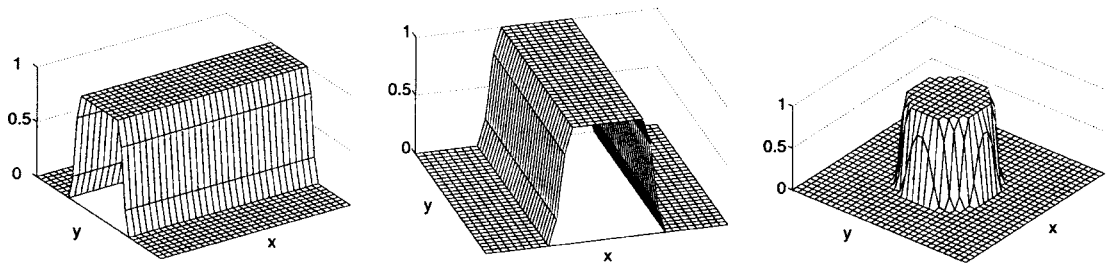

FIG. 5. Two-dimensional Π-modified functions (β=0.3, λ=0.2) to selectively filter horizontal edges in the y direction on the left, vertical edges in the x direction in the middle, and corners in both directions with a polar form on the right. The filters are respectively applied to acoustic fields H_1, V_1, and D_1 of Fig. 3 yielding the fields H_{1f}, V_{1f}, and D_{1f} of Fig. 6.

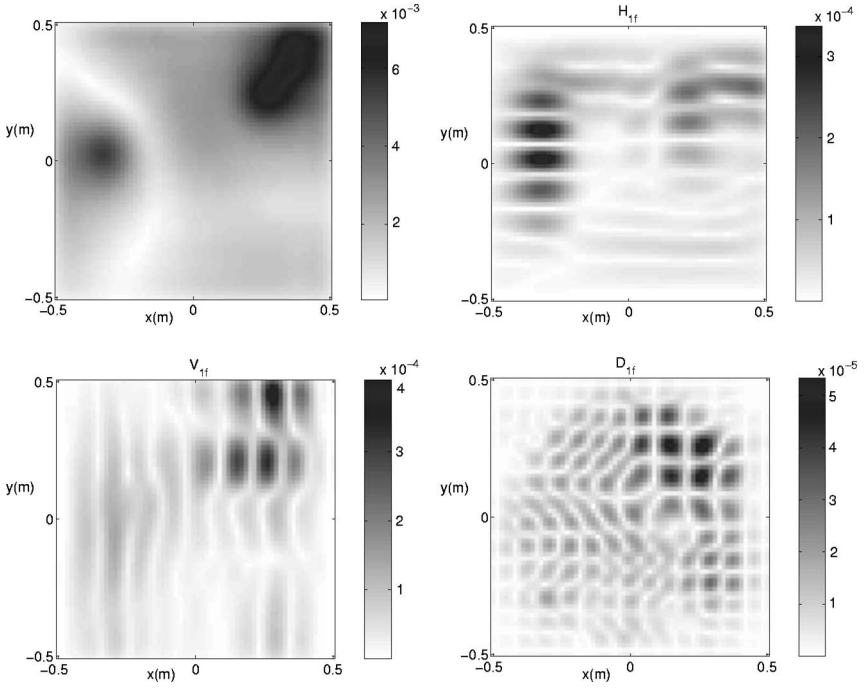

FIG. 6. Results (magnitude) of the filtering of the three detailed fields (H_1, V_1, D_1) in Fig. 3 by the Π-modified functions in Fig. 5 for horizontal edges top right (H_{1f}), vertical edges bottom left (V_{1f}), and corners bottom right (D_{1f}). The modulus of the modified acoustic field resulting from the addition of A_1, H_{1f}, V_{1f}, and D_{1f} is top left.

The three acoustic fields H_{1f}, V_{1f}, and D_{1f}, which result from selective spatial filtering near the borders of the antenna, are shown in Fig. 6. The strong edges have been removed, highlighting components that were masked before the selective filtering.

These three selectively filtered acoustic fields are then added to the approximation top left in Fig. 3 to give a new acoustic field $\hat{A}_1$ intended to be used as an input of the holography process (top left in Fig. 6):

$$\hat{A}_1 = A_1 + H_{1f} + V_{1f} + D_{1f}. \tag{3}$$

Figure 7 shows the wave number representation of the acquired pressure field 10 cm from the source plane (A_0) and the modified field resulting from the wavelet processing $(\hat{A}_1)$ to be presented to the NAH procedure. The modified acoustic field $\hat{A}_1$ results from a single resolution analysis. If wavelet preprocessing is performed at resolution j, the modified acoustic field $\hat{A}_j$ involves $3j+1$ subimages, $3j$ of which are spatially filtered, such that

$$\hat{A}_j = A_j + \sum_{i=1}^{j} (H_{if} + V_{if} + D_{if}). \tag{4}$$

IV. RESULTS FROM RECONSTRUCTED ACOUSTIC FIELDS

The back-propagation algorithm of standard NAH is run on either the acquired acoustic field 10 cm from the source plane or the modified pressure field of Eq. (4) resulting from the wavelet preprocessing. Figure 8 shows the reconstructed spatial acoustic fields 1 cm from the source plane from different configurations. Standard holography was investigated through the use of two filters in the wave number domain: the one proposed by Veronesi and Maynard[6] (also mentioned by Williams[5]), whose taper follows an exponential shape, and the one given by Li *et al.*,[19] derived from Veronesi's filter. The former is designed to eliminate too many propagative wave number components in the case of a weak slope at the break point. The two filters are tested with two cutoff wave numbers. The wavelet processing was performed for three resolutions, 1, 2, and 3. The influence of the size of the acquisition grid is also investigated. Whereas wavelet preprocessing always involves 16×16 pressure fields, standard holography is experimented on both 16×16 and 28×28 acoustic fields. Each calculation is made on a 32×32 grid. Indeed, the acquired fields are extended to 32×32 points by

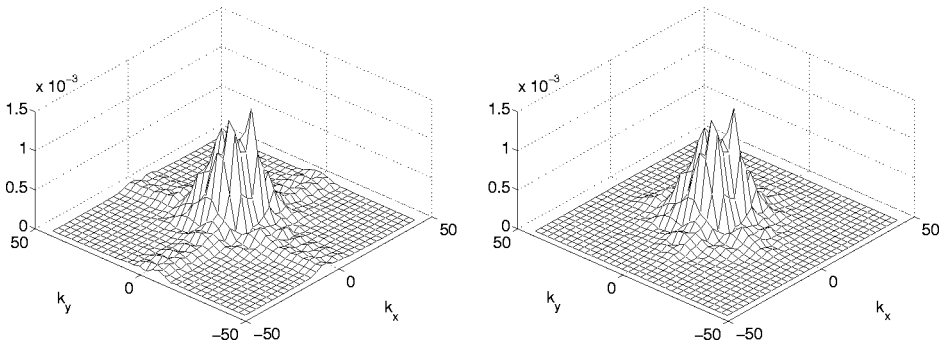

FIG. 7. K space representation (magnitude) of the acquired pressure field 10 cm from the source plane on the left and the modified field resulting from the wavelet processing on the right.

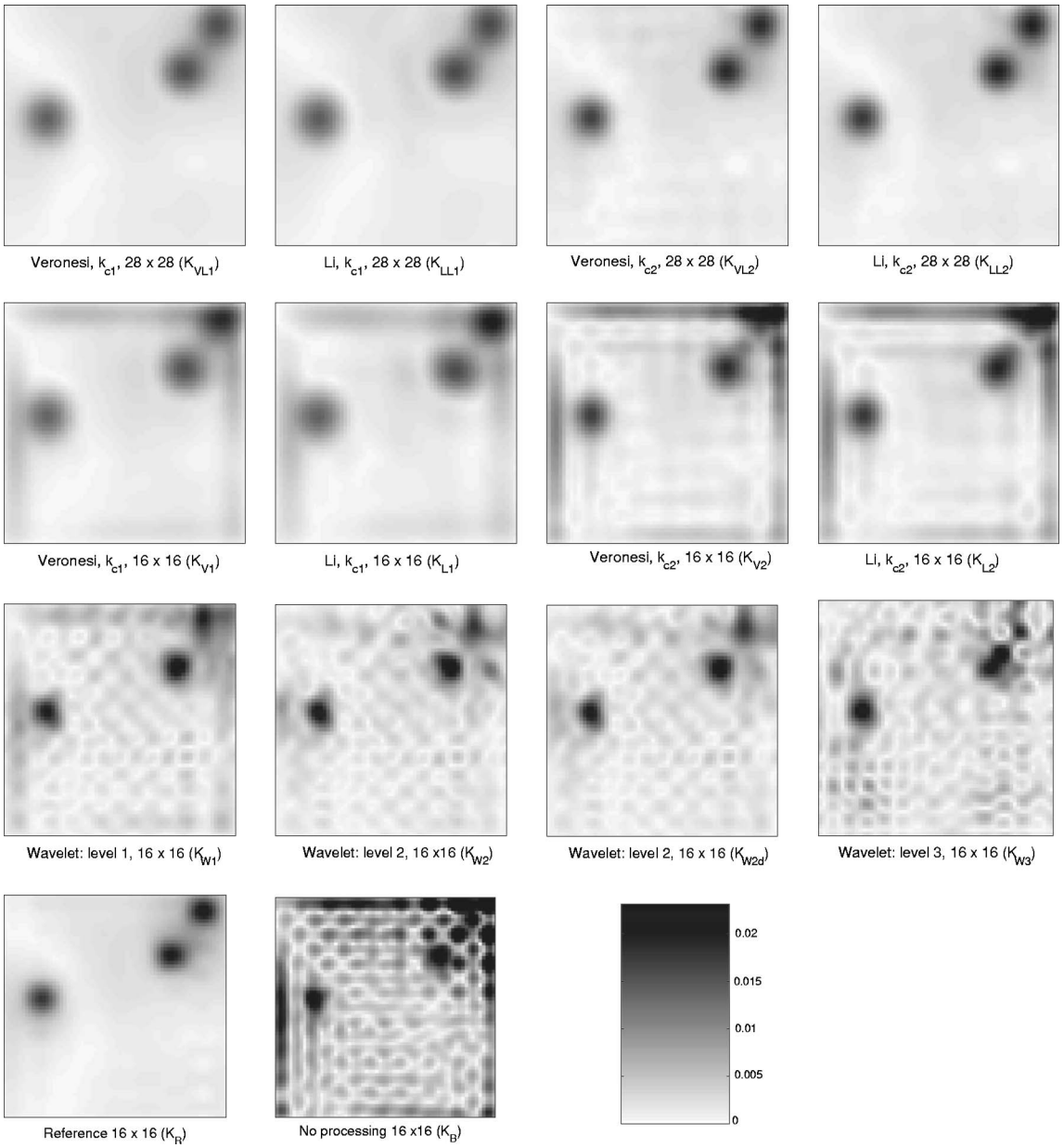

FIG. 8. Magnitudes of the reconstructed acoustic fields 1 cm from the source plane obtained from the acquired pressure field 10 cm from the loudspeaker plane. Each acoustic field obtained from standard NAH or wavelet processing can be compared to the reference one, bottom left, directly acquired 1 cm from the source plane. Each acoustic field is 1.0×1.0 m^2.

zero-padding corresponding to a 2.07×2.07 m^2 zone. However, the area of interest remains the 16×16 grid of dimension 1.0×1.0 m^2 shown in Fig. 8.

Finally, 14 reconstructed acoustic fields 1 cm from the source plane are shown:

(i) the reference acoustic field directly acquired 1 cm from the source plane,
(ii) the basic spatial field reconstructed from the acquired pressure field with no processing in k space,
(iii) eight spatial fields computed from the acquired pressure field 10 cm from the source plane and lessened by Veronesi or Li filtering with two different cutoff wave numbers $k_{c_1}=0.6k_{max}$ or $k_{c_2}=0.8k_{max}$, and
(iv) four spatial fields computed from the modified acquired pressure with a one-level, two-level, two-level with no spatial filtering of details, and three-level wavelet decomposition.

Every field has to be compared to the reference one at the bottom left of Fig. 8: the basic field obtained with no processing demonstrates the necessity to operate filtering in the wave number spectrum. The effects of Veronesi and Li filtering with the same cutoff wave number appear fairly similar: this is a known fact when the slope at the break point is steep. Acoustic fields computed from an extended area (28×28) logically do not exhibit distortion effects even if the sources are not as dark as those of the reference. By contrast, standard holography applied to a 16×16 grid leads to truncation effects at the edges, the sharpness of which

depends on the cutoff wave number. The cutoff wave number k_{c_1} is more satisfactory than k_{c_2}. Except for the third level decomposition, the fields resulting from the wavelet preprocessing give the best results: indeed, the three acoustic sources appear quite clearly and they are more confined and intense. The distortions due to the truncation of the antenna are smaller at level 2, compared to level 1. However, two dark spots can be seen on an equidistant line from the two up sources (see wavelet level two K_{W_2} in Fig. 8). These two points are due to overfiltering in the $[k_{max}/4, k_{max}/2]$ band. Indeed, the acoustic field back-propagated 1 cm from the sources, resulting from the method presented, when no detail filtering at level 2 is applied, does not reveal the spots (see wavelet level 2 $K_{W_{2d}}$ in Fig. 8).

V. EVALUATION OF THE VIABILITY OF THE METHOD

A. Introduction

Since the previous discussion was based on visual comparisons and since the acoustic fields resulting from the wavelet approach seem to show some background noise in Fig. 8, the conclusions may be arguable. In order to evaluate the viability of the wavelet method objectively, some indicators are necessary. We decided to compute the indicators on the wave number spectra (k spectra) taken before backward propagation which lead to the resulting spatial fields in Fig. 8. Indeed, the backpropagation algorithm is computed in the wave number domain for both standard holography and the wavelet approach (see Fig. 2). Furthermore, the k spectrum provides a powerful representation of the physics underlying the acoustic radiation of the sources of noise: the k spectrum separates the evanescent waves and the plane waves and highlights the directions of the plane waves radiated on the measurement plane.[20] The k spectrum is also used to compute acoustical velocity and, then, sound intensity.

That is why each k spectrum computed 10 cm from the source plane [yielding the reconstructed spatial acoustic fields 1 cm from the source plane (reported in Fig. 8)] is compared to the reference k spectrum K_R. This k spectrum is the two-dimensional Fourier transform of the pressure field directly acquired 1 cm from the source plane on a 16×16 grid, propagated by calculation at 10 cm. However, the visual comparison of the wave number spectra to the reference is not very clear, justifying why the spectra are not reported in the paper. Table I summarizes the notation and the characteristics of the wave number spectra K's. For the standard method, the first subscript denotes the type of the filter (V for Veronesi, L for Li) and the number denotes the cutoff wave number 1 for k_{c_1}, 2 for k_{c_2}. A capital L may appear when acquisition is made with a 28×28 "large" grid. For instance, K_{VL_1} denotes Veronesi filtering with the cutoff wave number k_{c_1} from a 28×28 grid extended to 32×32 by zero-padding. For the wavelet processing, the first subscript is W and the number indicates the level of the decomposition.

Two indicators are proposed for comparing these k spectra objectively: the first is based on similarity measurements between two wave number spectra, the second provides a relevant representation plane for the spectra where they are easy to compare.

B. Criteria for characterization

1. Similarity measurements

Thirteen wave number spectra K_P with P in $\{B, L_1, LL_1, L_2, LL_2, V_1, VL_1, V_2, VL_2, W_1, W_2, W_{2d}, W_3\}$ before backward propagation are compared to the reference K_R using several similarity measurements in the wave number domain $\mathcal{A}$, corresponding to the area covered by the array of measurement points. It is assumed that the minimum distance is obtained by the most relevant wave number spectrum. The similarity measurements are computed using the following distances, which Davy *et al.* used[21] for comparisons between time-frequency representations:

Manhattan distance

$$d_1(K_P,K_R)=\iint_{\mathcal{A}}|K_P(k_x,k_y)-K_R(k_x,k_y)|dk_x\,dk_y, \tag{5}$$

Euclidean distance

$$d_2(K_P,K_R)=\left[\iint_{\mathcal{A}}|K_P(k_x,k_y)-K_R(k_x,k_y)|^2\,dk_x\,dk_y\right]^{1/2}, \tag{6}$$

Correlation distance

$$d_{cor}(K_P,K_R)=\frac{[d_2(K_P,K_R)]^2}{\iint_{\mathcal{A}}|K_P(k_x,k_y)|^2\,dk_x\,dk_y+\iint_{\mathcal{A}}|K_P(k_x,k_y)|^2\,dk_x\,dk_y}, \tag{7}$$

Kolmogorov distance

$$d_{kol}(K_P^N,K_R^N)=\iint_{\mathcal{A}}|K_P^N(k_x,k_y)-K_R^N(k_x,k_y)|dk_x\,dk_y, \tag{8}$$

Küllback distance

$$d_{kul}(K_P^N,K_R^N)=\iint_{\mathcal{A}}[K_P^N(k_x,k_y)-K_R^N(k_x,k_y)]\times\log\frac{K_P^N(k_x,k_y)}{K_R^N(k_x,k_y)}\,dk_x\,dk_y, \tag{9}$$

Matusita distance

$$d_{mat}(K_P^N,K_R^N)=\sqrt{\iint_{\mathcal{A}}|\sqrt{K_P^N(k_x,k_y)}-\sqrt{K_R^N(k_x,k_y)}|^2\,dk_x\,dk_y}, \tag{10}$$

where the notation $K_P^N(k_x,k_y)$ emphasizes the normalization of the wave number spectrum:

$$K_P^N(k_x,k_y)=\frac{|K_P(k_x,k_y)|}{\iint_{\mathcal{A}}|K_P(k_x,k_y)|dk_x\,dk_y}. \tag{11}$$

Figure 9 shows the results obtained from the six different distance measurements defined above, between the reference and the studied wave number spectra. Full corresponding numerical results have already been reported.[22] Four distances (d_1, d_{kol}, d_{kul}, and d_{mat}) give almost the same positions and seem to validate the visual inspection from Fig. 8. Wave number spectra computed from a 28×28 grid are in general more accurate than those computed from a 16×16

TABLE I. Review of the wave number spectra to compare. MA_i means multiresolution analysis of level i. $K_{W_{2d}}$ is different from K_{W_2} by the fact that the modified pressure field at resolution 2 is computed with no filtering of the corners.

Wave number spectrum		Grid		Processing
Reference K_R		16×16		no
K_B		16×16		no
K_{L_1}	K_{LL_1}	16×16	28×28	Li (0.6 k_{max})
K_{L_2}	K_{LL_2}	16×16	28×28	Li (0.8 k_{max})
K_{V_1}	K_{VL_1}	16×16	28×28	Veronesi (0.6 k_{max})
K_{V_2}	K_{VL_2}	16×16	28×28	Veronesi (0.8 k_{max})
K_{W_1}	K_{W_3}	16×16		MA_1 MA_3
K_{W_2}	$K_{W_{2d}}$	16×16		MA_2

grid. The spectra obtained by the wavelet preprocessing at resolution 2 are the closest to the reference, whatever the distance used. However, these distance measurements have the disadvantage of comparing two images pixel by pixel. Therefore they are very sensitive to the position of the pressure field maxima.

2. A representative space for comparing k spectra

The aim of this approach is to associate a representative pattern with each of the 14 k spectra in Table I. In pattern recognition, a pattern is composed of d real numerical components and may then be represented by a point in the feature space $\mathbb{R}^d$. Two patterns are similar if the distance between them is short in the feature space. For the purposes of the study, the patterns are composed of the marginal wave number distribution, extracted from a k spectrum, which gives information about the relative positions of the wave numbers.

The marginal wave number distributions $E_x(k_x)$ and $E_y(k_y)$, respectively along k_x and k_y directions of the wavenumbers $K_P(k_x,k_y)$, are defined as

$$E_x(k_x) = \frac{\int_{\mathcal{A}} |K_P(k_x,k_y)|\,dk_y}{\iint_{\mathcal{A}} |K_P(k_x,k_y)|\,dk_x\,dk_y}, \tag{12}$$

$$E_y(k_y) = \frac{\int_{\mathcal{A}} |K_P(k_x,k_y)|\,dk_x}{\iint_{\mathcal{A}} |K_P(k_x,k_y)|\,dk_x\,dk_y}. \tag{13}$$

Figure 10 shows the marginal wave number distribution along k_x for several k spectra including the reference K_R. In comparison with K_R, K_{W_2} behaves well in [5, 20], as does K_{V_1} in [32, 44]. Wave numbers seem to be overfiltered in [5, 10] with wavelet processing at level 3, and underfiltered in [10, 30] at level 1. These effects are consistent with multiresolution analysis properties reported in Sec. III B. The impression of accuracy given by the reconstructed acoustic field 1 cm from the sources from a second level multiresolution analysis (Fig. 8) may be explained by the filtering operated in the [5, 20] band.

In the study, the patterns are composed of 64 components, given by both distributions E_x and E_y (32 for each one). Therefore the feature space is $\mathbb{R}^{64}$. It is obviously not appropriate to represent the 14 patterns in the feature space. Thus a principal component analysis (PCA) is performed on the pattern set to reduce the dimension of the representation space. It allows us to project the patterns on an orthogonal basis with two axes obtained by linear combination of the input features. This representation gives information about the similarities between the wave number spectra studied. The results are reported in Fig. 11. The projection made by the PCA led to a loss of information of 22%, which is sufficient to validate the representation.

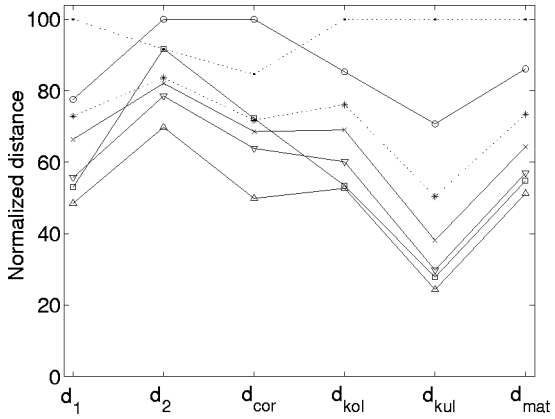

FIG. 9. Six distance measurements (Manhattan d_1, Euclidean d_2, Correlation d_{cor}, Kolmogorov d_{kol}, Küllback d_{kul}, Matusita d_{mat}) between the reference wave number spectrum K_R and the spectra K_B (dotted .), K_{W_3} (○), K_{V_2} (dotted ∗), K_{W_1} (×), K_{V_1} (▽), K_{VL_1} (□), and $K_{W_{2d}}$ (△). For each distance measurement, the longest distance is set to value 100. The distance measurements involving K_{L_1}, K_{L_2}, and K_{W_2} are not represented because they are respectively close to those involving K_{V_1}, K_{V_2}, and $K_{W_{2d}}$. It is the same for the distance measurements involving K_{LL_1}, K_{LL_2}, and K_{VL_2} that are similar to the measurement concerning K_{VL_1}.

Considering the PCA plane in Fig. 11, the marginal distribution seems to be a relevant feature. K_{W_2} and $K_{W_{2d}}$ are seen to behave very well: they are located near the reference. The similarities between Veronesi and Li filtering and the distance from K_B and the other points may also be noticed. The spectra computed from a large grid are the closest to the reference. In conclusion, an examination of the projection in the plane of the 14 patterns (see Fig. 11), provided by the wave number spectra studied, seems to give the same impression as the visual analysis of the reconstructed acoustic fields of Fig. 8. It confirms that the results obtained from the wavelet preprocessing for resolution 2 appeared more accurate than those given by standard holography with Veronesi or Li filtering. Furthermore, the marginal wave number distribution is established as a relevant feature for characterizing wave number spectra.

VI. CONCLUSIONS

We have demonstrated the relevance of wavelet preprocessing applied to the acquired pressure field in the nearfield of stationary sources before back-propagation by standard NAH. The method may also be used in a nonstationary context. In this context, the constraint is based particularly on the fact that the microphones of the array must operate simultaneously.

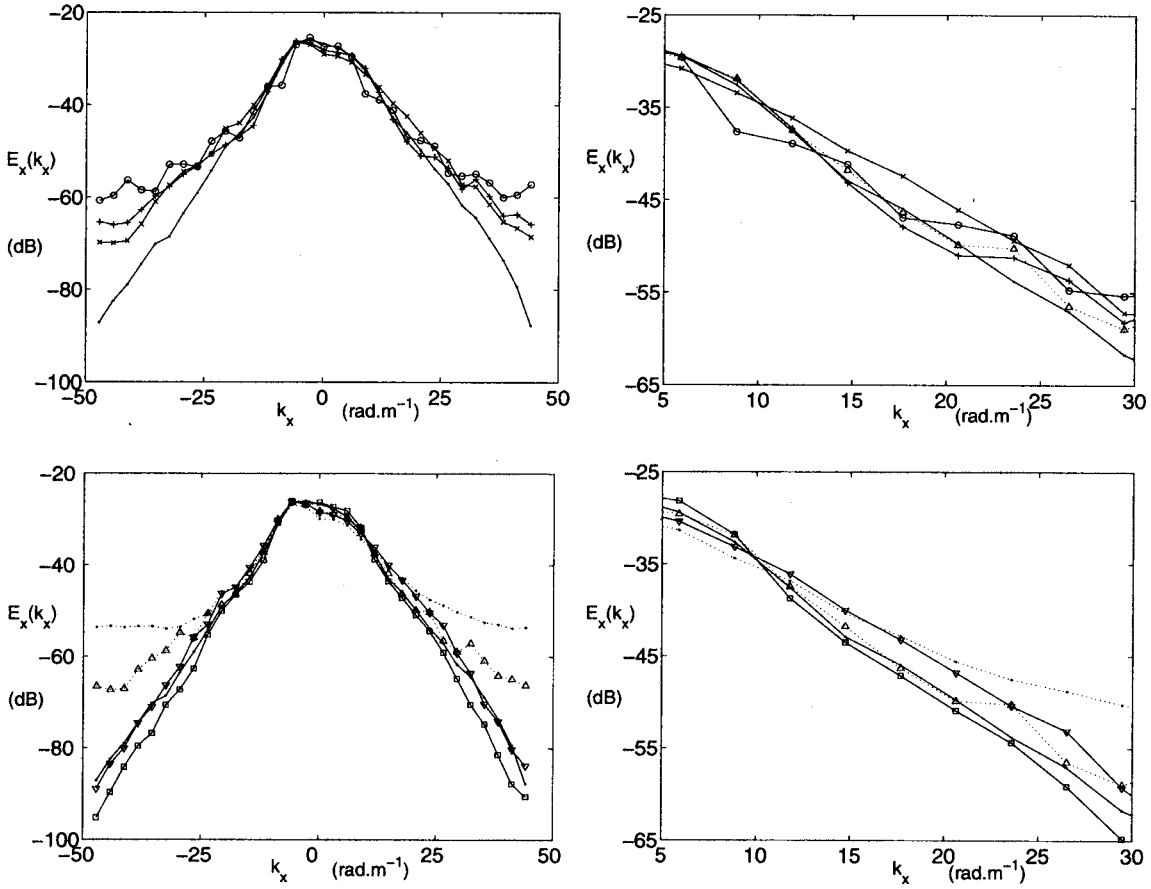

FIG. 10. Marginal wave number distribution $E_x(k_x)$ in decibels for k-spectra K_R (solid .), K_{W_1} ($\times$), K_{W_2} ($+$), K_{W_3} ($\bigcirc$), $K_{W_{2d}}$ (dotted $\triangle$), K_B (dotted .), K_{V_1} ($\triangledown$), and K_{VL_1} ($\square$) with zoom in on [5 30] on the right.

The wavelet method is to be considered as a preprocessing routine which is appropriate to lessen the effects due to the truncation of the hologram. It does not enter into competition with other methods working in the wave number domain, but rather in complement to these methods. From this point of view, wavelet preprocessing could be used in conjunction with regularization techniques; patch formulation, in particular, because the wavelet technique does not take into account the backward propagation distance and its influence on evanescent waves. However, wavelet processing is particularly effective for reducing distortion due to the truncation of acoustic fields because it works selectively in space and wave number domains. The methods of regularization are, on the other hand, built from a noisy k spectrum model, thus particularly effective in the case of measurement noise.

Furthermore, the pattern recognition approach we used to compare the wavelet method to standard NAH demonstrates the relevance of wave number marginal distribution which provides an objective criterion to assess the viability of wavelet preprocessing. Experimentation using this approach may well prove the relevance of any processing method involving acoustic field images.

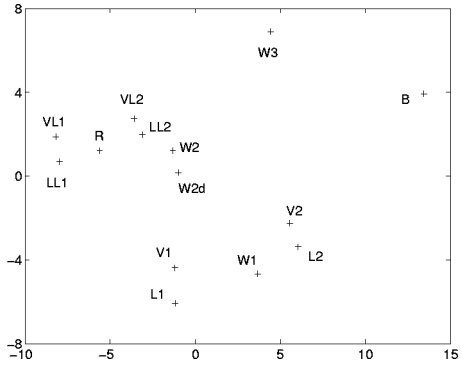

FIG. 11. Representative space for comparing patterns composed of wave number marginal distribution, resulting from principal component analysis (78% information kept).

[1]H. S. Kwon and Y. H. Kim, "Minimization of bias error due to windows in planar acoustic holography using a minimum error window," J. Acoust. Soc. Am. **98**, 2104–2111 (1995).
[2]P. A. Nelson and S. H. Yoon, "Estimation of acoustic source strength by inverse methods: Part i, conditioning of the inverse problem," J. Sound Vib. **233**, 643–668 (2000).
[3]S. H. Yoon and P. A. Nelson, "Estimation of acoustic source strength by inverse methods: Part ii, experimental investigation of methods for choosing regularization parameters," J. Sound Vib. **233**, 669–705 (2000).
[4]J. Hald, "Reduction of spatial windowing effects in acoustical holography," Proceedings of Inter-Noise 94, Yokohama, Japan, 29–31 August 1994, pp. 1887–1890.
[5]E. G. Williams, "Regularization methods for near-field acoustical holography," J. Acoust. Soc. Am. **110**, 1976–1988 (2001).
[6]W. A. Veronesi and J. D. Maynard, "Nearfield acoustic holography (NAH): II. Holographic reconstruction algorithms and computer implementation," J. Acoust. Soc. Am. **81**, 1307–1322 (1987).
[7]A. Schuhmacher, J. Hald, K. B. Rasmussen, and P. C. Hansen, "Sound source reconstruction using inverse boundary element calculations," J. Acoust. Soc. Am. **113**, 114–127 (2003).
[8]X. Zhao and S. F. Wu, "Reconstruction of vibro-acoustic fields using

hybrid nearfield acoustic holography," J. Sound Vib. **282**, 1183–1199 (2005).
[9]E. G. Williams, "Continuation of acoustic near-fields," J. Acoust. Soc. Am. **113**, 1273–1281 (2003).
[10]E. G. Williams, B. H. Houston, and P. C. Herdic, "Fast Fourier transform and singular value decomposition formulations for patch nearfield acoustical holography," J. Acoust. Soc. Am. **114**, 1322–1333 (2003).
[11]J. R. F. Arruda, "Surface smoothing and partial spatial derivatives computation using a regressive discrete Fourier series," Mech. Syst. Signal Process. **6**, 41–50 (1992).
[12]J.-C. Pascal, J.-F. Li, and X. Carniel, "Wavenumber processing techniques to determine structural intensity and its divergence from optical measurements without leakage effects," Shock Vib. **9**(1-2), 57–66 (2002).
[13]Z. El-Khoury and C. Nouals, "Utilisation de l'analyse multirésolution en holographie acoustique champ proche," (Acoustic holography using wavelet transform), Trait. Signal **11**, 257–270 (1994).
[14]J.-H. Thomas and J.-C. Pascal, "Using wavelets to reduce distortion problems in near field acoustic holography," Proceedings of Inter-Noise 01, The Hague, The Netherlands, 27–30 August 2001, pp. 2175–2178.
[15]J.-H. Thomas and J.-C. Pascal, "Acoustic holography experiments using a wavelet preprocessing method," Proceedings of ISMA 2002, Leuven, Belgium, 16–18 September 2002, pp. 1825–1833.
[16]S. Mallat, *A Wavelet Tour of Signal Processing* (Academic, New York, 1998).
[17]M.-H. Masson, B. Dubuisson, and C. Frélicot, "Conception d'un module de reconnaissance des formes floue pour le diagnostic," (Design of a fuzzy pattern recognition system for the diagnosis), J. Eur. Syst. Automat. (RAIRO-APII-JESA), 319–341 (1996).
[18]I. Daubechies, "Ten Lectures on Wavelets," Regional Conference Series in Applied Mathematics, SIAM (1992).
[19]J. F. Li, J.-C. Pascal, and C. Carles, "A new K-space optimal filter for acoustic holography," Proceedings of the 3rd International Congress on Air and Structure Borne Sound and Vibration, Montreal, Canada, 13–15 June 1994, pp. 1059–1066.
[20]E. G. Williams, *Fourier Acoustics* (Academic, New York, 1999).
[21]M. Davy, C. Doncarli, and G. F. Boudreaux-Bartels, "Improved optimization of Time-frequency based signal classifiers," IEEE Signal Process. Lett. **8**(2), 52–57 (2001).
[22]J.-H. Thomas and J.-C. Pascal, "A study of the relevance of an acoustic holography method using wavelets based on features extracted from wavenumber spectra," Proceedings of Inter-Noise 03, Jeju, Republic of Korea, 25–28 August 2003, pp. 2667–2674.